Damage Assessment of Casting Materials in High Temperature Applications Influenced by Varying Plasticity Models

F. Laengler[1], K. Naumenko[2]

[1]BorgWarner Turbo Systems Engineering GmbH, Kirchheimbolanden, Germany

[2]Institue of Mechanics, Otto-von-Guericke University of Magdeburg, Germany

Abstract: The turbine housing of an exhaust turbocharger is exposed to extensive cyclic thermo-mechanical loading. Consequently, the design of the turbine housing becomes a major challenge in ensuring the guaranteed lifetime in relation to the high-temperature behavior of the materials. In a first step, a phenomenological lifetime approach together with a rate-independent constitutive plasticity model of Chaboche-type was developed and validated for application on casting materials. The present study deals with the more detailed analysis of rate-dependent plasticity applied in the finite-element analysis with respect to the subsequent creep-fatigue damage calculation procedure. For capturing time-dependent effects both a creep law was additively superimposed to the rate-independent plasticity model and a constitutive viscoplastic model was developed for the casting material Ni-resist D5S. The creep model is by default implemented in Abaqus, whereas the viscoplastic model has to be linked via the programming interface. Thermomechanical fatigue tests on specimens under characteristic load conditions have been used to validate the influence of these different kinds of material models when describing the deformation behavior. Lifetime estimations are strongly dependent on the finite-element analysis output variables, and furthermore, the damage calculation procedure itself has to conform to the phenomena previous modeled.

Keywords: Plasticity, Creep, Low-Cycle Fatigue, Damage, Thermomechanical Fatigue, Thermal Stress, Ni-resist D5S.

1. Introduction

The most cost-intensive key component of an exhaust turbocharger is the turbine housing (T/H) that provides the kinetic energy required for charging. Inhomogeneous temperature distributions and the interaction with neighboring components constrain the thermal expansion and contraction of the T/H, thus causing local multiaxial stress states with inelastic strains during operation. Numerous test stand runs are generally needed in order to find the appropriate combination of the complex design and material. On the one hand, functionality without leakage must be ensured during the guaranteed service life and, on the other, customer requirements together with the installation space need to be met. Hence, there is a demand for reliable calculation methods allowing lifetime assessment with respect to thermo-mechanical fatigue (TMF) early in the design process. Such TMF methods are essential, for instance to employ the full potential of materials and also to reduce the material costs as well as the effort for component testing by better understanding the cyclic mechanical long-term behavior at elevated temperatures. Improvements in this respect could be shown in terms of coupling the numerical component structural analysis with a validated phenomenological lifetime approach based on creep-fatigue damage assessment (Laengler, 2010a,b). The constitutive material model of Chaboche-type applied in a preceding finite-element analysis (FEA) describes the rate-independent elastoplastic material behavior. Thus, time-dependent phenomena such as creep strain and stress relaxation, which are essential for creep damage, are subsequently recalculated within the lifetime approach. Such recalculation procedures are based not only on several assumptions, but also stress and strain redistributions caused by the complete component behavior are not considered due to locally and independently performed corrections.

Unquestionably, the quality of the lifetime approach is strongly dependent on the preceding FEA. Besides transient thermal boundary conditions and the FE model setup, the material model applied in the FEA determines both the quantity of the result variables which serve as input variables for the subsequent damage calculation and the structure of the calculation method itself, i.e. which damage-specific phenomena are considered or have to be recalculated. The material model as an important key feature of the component structural analysis is of special interest in this work. The influence of an extended material model applied in the FEA is investigated to describe the deformation behavior. For that purpose a creep law is additively superimposed to the rate-independent plasticity model of Chaboche-type mentioned in e.g. (Laengler, 2010a). The plasticity model, as well as the creep model, are by default implemented in Abaqus. In addition, a constitutive viscoplastic model was developed which has to be linked via the programming interface to Abaqus. Both extended material model variants are calibrated and applied to the casting material Ni-resist D5S. In order to use uniquely determined stress and strain states, TMF tests on specimens under characteristic load conditions have been used for comparison reasons. Due to the capturing of time-dependent phenomena by the extended material model in the FEA, the subsequent damage calculation method has to be modified. Any corrections with respect to creep strain and stress relaxation are no longer required. Thus, the limiting material-specific creep-fatigue damage value needs to be revalidated for future T/H applications.

2. Component structural analysis

2.1 Modus operandi

The modus operandi of the T/H design evaluation process is shown in Figure 1. Due to the variety of different T/H materials used in passenger car and commercial diesel applications, the cost-benefit ratio is an important requirement and has to be allowed for. Consequently, an efficient level of effort taken in both determining required material-dependent parameters and numerical calculation of entire turbocharger models, including computational fluid dynamics (CFD) and heat transfer calculation, is essential to keep the evaluation time as flexible as necessary. For that purpose, the constitutive material model is one of the limiting factors. The more physical phenomena can be captured by the model, the more effort is usually necessary. Experimental results of thermal shock tested T/H's serve as the reference to assess the calculated thermo-mechanical T/H behavior under tightened load conditions for accelerated testing.

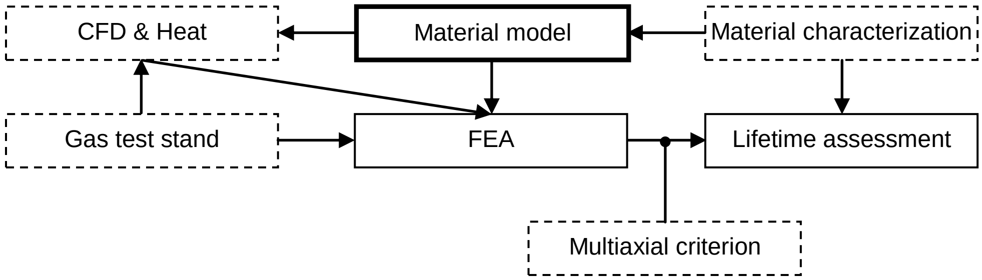

Figure 1. Modus operandi applied for the evaluation of the T/H design with respect to different types of materials.

The results of the FEA in terms of time series are in general fully 3-dimensional. But the lifetime approach afterwards requires 1-dimensional input quantities. Therefore, it is inevitable to evaluate an adequate reduction method to handle the multiaxiality for casting materials. The equivalent 1-dimensional input variables of 3-dimensional tensors have to be defined in such a manner that the lifetime estimations are of acceptable accuracy. The multiaxial criterion depends strongly on the material's ductility/brittleness. Among other evaluated energy criteria, the critical plane approach defined by maximum normal stress fulfills this requirement in a first step.

2.2 Material Ni-resist D5S

The material investigated in this work is an austenitic nodular graphite cast iron of type Ni-resist D5S. Its chemical decomposition is given in Table 1. T/H's are complex castings of predominantly thin section requiring a demanding combination of properties. D5S as a highly castable iron provides the required combination of properties, e.g. ductility together with relatively hot strength as well as low coefficient of thermal expansion to resist high temperature gradients. D5S is finding application up to maximum exhaust gas temperature of 950°C.

Table 1. Chemical composition of D5S.

Chemical element, % by mass						
C	**Si**	**Mn**	**S**	**P**	**Ni**	**Cr**
≤ 2.4	1.5-3.0	0.5-1.0	≤ 0.02	≤ 0.08	34.0-36.0	2.0-3.0

For high temperature applications under reversal load conditions not only the cyclic material behavior, but also time-dependent phenomena like creep and relaxation, are of interest. The technical yield limit ($R_{p0.01}$) of the cyclic stabilized material condition together with the isochronous creep rupture strength after 1000 hours ($R_{m/1000h}$) are shown in Figure 2. Starting at approx. 500°C, a creep rupture after 1000 hours can be expected caused by purely elastic stress.

Thus, it is essential that fatigue damage and, in addition, creep damage or also their interaction are taken into account for lifetime assessment by ensuring the functionality of the T/H during operating time.

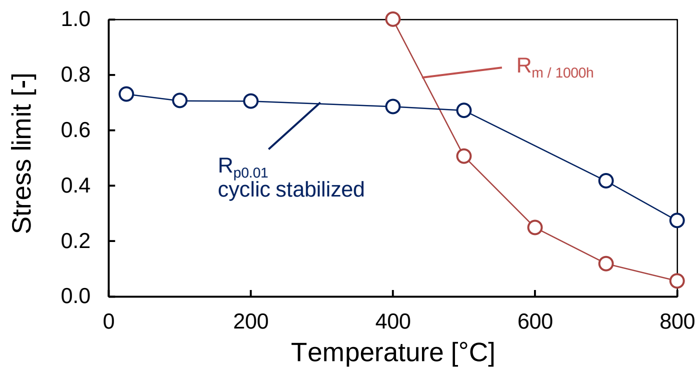

Figure 2. Standardized technical yield limit $R_{p0.01}$ and isochronous creep rupture strength $R_{m/1000h}$ of D5S.

2.3 Material models

2.3.1 Elastoplastic model

By default, lifetime assessment was evaluated by applying a constitutive material model which is based on the work of Chaboche (Chaboche, 1986, 1989) and describes rate-independent elastoplasticity. The temperature-dependent formulation of this model is implemented in Abaqus (Abaqus Theory Manual). Phenomena typical for materials subject to cyclic loading, in which plastic strain does continuously reverse direction sharply, can be modeled, as is typically the case in the turbine housing due to the alternating heating-up and cooling-down phases.

The incremental mechanical equations of the material model are given in Table 2. Mechanical strain rate tensor $d\boldsymbol{\varepsilon}$ in Equation (1) is a linear combination of the reversible elastic part $d\boldsymbol{\varepsilon}_e$ and the irreversible solely plastic part $d\boldsymbol{\varepsilon}_p$. The total strain is a superposition of the mechanical strain and the thermal strain. The latter is calculated by use of the linear thermal expansion coefficient multiplied by temperature change. Stress tensor $\boldsymbol{\sigma}$ is determined on the basis of the elasticity tensor $\mathbf{a}$ that depends on temperature T and consists of the elastic constants, Equation (2). The plastic strain is defined by the assumed associated flow rule, Equation (3), whereby dp represents the accumulated plastic strain rate. The pressure-independent von Mises yield function f allowing for kinematic hardening is defined by Equation (4), whereby $J(\boldsymbol{\sigma}\text{-}\mathbf{X})$ denotes the distance in the deviatoric stress space. Deviatoric parts of backstress $\mathbf{X}$' and of stress tensor $\boldsymbol{\sigma}$' are included in the conditional Equation (5). The initial size of the yield surface at zero plastic strain k remains constant for a certain temperature through the neglect of isotropic hardening. The non-isothermal and non-linear incremental evolution law of the strain valued backstress component $\mathbf{X}_k$ is formulated in Equation (6). C_i and γ_i are temperature-dependent material parameters.

Table 2. Constitutive mechanical part of the elastoplastic material model.

$$d\boldsymbol{\varepsilon} = d\boldsymbol{\varepsilon}_e + d\boldsymbol{\varepsilon}_p \tag{1}$$

$$\boldsymbol{\sigma} = \mathbf{a} : \boldsymbol{\varepsilon}_e \tag{2}$$

$$d\boldsymbol{\varepsilon}_p = dp \frac{\partial f}{\partial \boldsymbol{\sigma}} \ , \ dp = \sqrt{\frac{2}{3} d\boldsymbol{\varepsilon}_p : d\boldsymbol{\varepsilon}_p} \tag{3}$$

$$f = J\left(\boldsymbol{\sigma} - \mathbf{X}\right) - k = 0 \tag{4}$$

$$J\left(\boldsymbol{\sigma} - \mathbf{X}\right) = \sqrt{\frac{3}{2}\left(\boldsymbol{\sigma}' - \mathbf{X}'\right) : \left(\boldsymbol{\sigma}' - \mathbf{X}'\right)} \tag{5}$$

$$d\boldsymbol{X}_i = C_i \frac{1}{k}\left(\boldsymbol{\sigma} - \boldsymbol{X}\right) dp - \gamma_i \boldsymbol{X}_i dp + \frac{1}{C_i} \frac{\partial C_i}{\partial T} \boldsymbol{X}_i dT \ , \ d\boldsymbol{X} = \sum\nolimits_{i=1}^{2} d\boldsymbol{X}_i \tag{6}$$

In terms of parameter identification, especially concerning kinematic hardening, only the cyclic stabilized elastoplastic material condition at mid-life is of interest. This results in several datasets of best-fitted parameters, each assigned to a given temperature. In the case of anisothermal calculations, the parameter set required for a certain temperature has to be interpolated between the underlying datasets.

2.3.2 Elastoplastic & creep model

To cover time-dependent deformation, a creep strain component is added to the purely elastoplastic model introduced before. It is assumed, that both inelastic strain components, plastic strain and creep strain, are uncoupled of each other (Abaqus Theory Manual). Hence, each inelastic strain variable is calculated separately by Abaqus such that the mechanical strain rate tensor introduced in Equation (1) consists of one more superimposed component, the creep strain rate $d\boldsymbol{\varepsilon}_c$:

$$d\boldsymbol{\varepsilon} = d\boldsymbol{\varepsilon}_e + d\boldsymbol{\varepsilon}_p + d\boldsymbol{\varepsilon}_c \ . \tag{7}$$

The creep strain rate is formulated similar to the Norton-Bailey power law (Norton, 1929) describing secondary creep by assuming time hardening. The power law formulation contains the deviatoric part of stress tensor $\boldsymbol{\sigma}$'.

$$d\boldsymbol{\varepsilon}_c = A\left(\boldsymbol{\sigma}'\right)^n t^m \tag{8}$$

The parameter set A, n, m is optimized in each case for a given sampling temperature of creep tests conducted to represent varying stress.

To provide the creep law, in addition to the non-linear kinematic hardening plasticity model by neglecting isotropic hardening described in chapter 2.3.1, the Abaqus material input file has to be formulated as follows:

```
*MATERIAL, NAME=name
⋮
*PLASTIC, HARDENING=combined, DATA TYPE=parameters, NUMBER BACKSTRESSES=2
k1, C11, γ11, C12, γ12, T1
k2, C21, γ21, C22, γ22, T2
⋮
ki, Ci1, γi1, Ci2, γi2, Ti
*CREEP, LAW=strain
A1, n11, m11, T1
A2, n21, m21, T2
⋮
Aj, nj1, mj1, Tj
```

The number of sampling temperatures i and j, at which parameter sets for the plastic model as well as for the creep model are available, are independent of each other. As can be seen in Figure 2, D5S indicates a more relevant creep influence starting at approx. 500°C, whereby the plasticity model needs to be fully characterized within the entire temperature range required by the FEA. The creep strain calculation is activated by using the keyword ***VISCO** together with its settings in the step section of the simulation input file.

2.3.3 Viscoplastic model

A viscoplastic material model that reflects inelastic behavior in a wide stress, strain rate and temperature range is developed and utilized inside Abaqus via the programming interface. The model includes the constitutive equation for the inelastic strain rate tensor, Equation (9).

$$\mathrm{d}\boldsymbol{\varepsilon}_{\mathrm{p}} = \frac{3}{2}\frac{\mathrm{d}\varepsilon_{\mathrm{vM}}}{\bar{\sigma}_{\mathrm{vM}}}\left(\boldsymbol{\sigma}'-\mathbf{X}'\right) \tag{9}$$

$$\bar{\sigma}_{\mathrm{vM}} = \sqrt{\frac{3}{2}\mathrm{tr}\left[\left(\boldsymbol{\sigma}'-\mathbf{X}'\right):\left(\boldsymbol{\sigma}'-\mathbf{X}'\right)\right]}$$

$$\mathrm{d}\varepsilon_{\mathrm{vM}} = R\left(\mathrm{T}\right) f\left(\bar{\sigma}_{\mathrm{vM}}\right)$$

The active equivalent von Mises stress $\bar{\sigma}_{\mathrm{vM}}$ is defined by the deviatoric part of stress tensor $\boldsymbol{\sigma}'$ and backstress tensor $\mathbf{X}'$, respectively. The equivalent von Mises strain rate $\mathrm{d}\varepsilon_{\mathrm{vM}}$ comprises a response function of temperature $R(\mathrm{T})$ and a response function of stress $f(\bar{\sigma}_{\mathrm{vM}})$.

$$\mathrm{d}\mathbf{X}' = \frac{1}{\mu\left(\mathrm{T}\right)}\frac{\mathrm{d}\mu}{\mathrm{dT}}\mathrm{dT}\ \mathbf{X} + \frac{2}{3}\mu\left[\mathrm{d}\boldsymbol{\varepsilon}_{\mathrm{p}} - \frac{3}{2}\mathrm{d}\varepsilon_{\mathrm{vM}}\frac{\mathbf{X}}{h\left(\sigma_{\mathrm{vM}},\mathrm{T}\right)}\right] \tag{10}$$

In Equation (10) the evolution law for the backstress deviator as proposed by Armstrong and Frederick (Armstrong, 1966) is given; μ(T) represents a response function of temperature, $h(\sigma_{vM},T)$ a response function of stress and temperature.

To characterize the strain rate sensitivity in a wide stress range, the Garofalo-type response function (Garofalo, 1965) of the von Mises equivalent stress σ_{vM} is applied. To capture the temperature dependence, a response function with two values of the activation energy for low and high temperature levels is proposed. Master curves for the normalized strain rate as a function of the normalized stress for the entire temperature range illustrate that the applied response functions characterize the material behavior with a satisfactory accuracy. Furthermore, the hardening behavior for both creep and low-cycle fatigue (LCF) regimes are well reproduced by the model. One feature of the developed approach is a relatively small number of material parameters and response functions if compared to the available unified constitutive models of viscoplasticity.

2.4 Lifetime approach

The lifetime assessment is based on an empiric phenomenological approach, see e.g. (Scholz, 2005), to estimate the number of cycles until crack initiation N_f. The approach is strain-based and assumes a defect-free material with a behavior like specimens in LCF tests and time-to-rupture tests. By applying the life fraction rule (Taira, 1962) for creep/relaxation and Miner's rule (Miner, 1945) for fatigue, failure is determined by the cycle at mid-life in terms of the summation of creep damage L_t and fatigue damage L_A, wherein both failure fractions are assumed to be approximately independent of each other. The damage evaluation follows Equation (11) resulting in the material-specific creep-fatigue damage sum L.

$$L_t + L_A = N_f \left(\sum_j \frac{\Delta t_j(\sigma_j)}{t_u(\sigma_j)} + \frac{1}{N_f^0} \right) = L \qquad (11)$$

Creep damage is calculated with respect to the variation of stress during a cycle. When fulfilling the creep condition at an individual time step/increment j during a cycle, the quotient of the corresponding time interval length $\Delta t_j=t_j-t_{j-1}$ and the rupture time t_u of the effective acting stress σ_j is calculated. It is assumed that tensile and compressive stress both have an equal effect on creep, and no distinction is made when calculating the creep damage.

Time-to-rupture tests at several sampling temperatures T with respect to varying load levels are used to describe the creep behavior as well as the creep damage. To avoid interpolation between different time-to-rupture curves and to compensate the scattering of experimental results, the Larson-Miller time-temperature parameter P_{LM} (Larson, 1952) containing a material-specific calibration factor C is applied:

$$P_{LM} = (273+T)\left(C + \log(t_u)\right) \ . \qquad (12)$$

The rupture time is derived from the master curve by solving the parameter definition in Equation (12). Experimental data are used to fit the master curve by applying a polynomial law within the typical application range for creep damage calculation, see Figure 3.

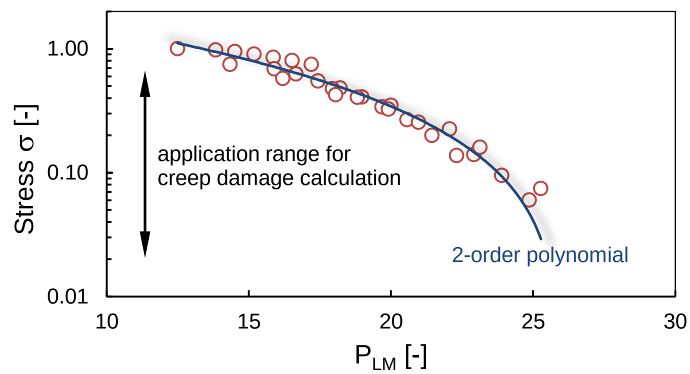

Figure 3. Standardized stress vs. Larson-Miller parameter P_{LM} for D5S.

In the case of fatigue damage, it is proposed that the LCF life curves at maximum cycle temperature T_{max} and minimum cycle temperature T_{min} together with the maximum strain width range $\Delta\varepsilon_{max}$ be considered. In order to calculate a geometric temperature-dependent mean value of fatigue life N_f^0 at mid-life, the empirical relationship in Equation (13) is introduced.

$$\frac{1}{N_f^0} = \frac{1}{2}\left[\frac{1}{N_f\left(\Delta\varepsilon_{max}, T_{max}\right)} + \frac{1}{N_f\left(\Delta\varepsilon_{max}, T_{min}\right)}\right] \tag{13}$$

Depending on the kind of material model applied in the FEA, effective stress and strain values have to be calculated before damage assessment. The recalculation of both creep strain and stress relaxation are required in the case of the purely elastoplastic material model of chapter 2.3.1, whereby this procedure is explicit described in (Laengler, 2012).

3. TMF damage assessment

3.1 TMF testing

In terms of damage evaluation and validation of the lifetime approach, a test series of in-phase TMF tests under characteristic load conditions was performed in a special TMF test rig at the Technical University of Darmstadt, Institute for Materials Science. Smooth material specimens of D5S with a diameter of 10.0 mm and gauge length of 19.94 mm were used. The significant TMF loading history was derived on the surface of T/H critical positions as results of the FEA; temperature and strain vs. time sequences are in accordance with Figure 4. The total strain is additively decomposed in a thermal and mechanical part. Strain width range values in axial direction are standardized on the maximum appearing value.

The underlying specimen temperature from approx. 220°C up to above 720°C was measured by a spot-welded thermocouple located in the transitional part of the specimen. In addition, temperature at the centre of the testing zone was recorded by a pyrometer. Temperature induced axial thermal strain was measured prior to start of cycle sequence in strain control mode to enable thermal strain compensation during testing. Axial strain was measured by side contact extensometer.

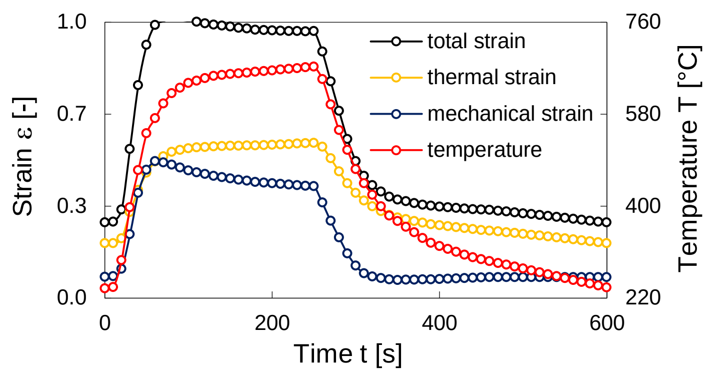

Figure 4. TMF load sequences.

3.2 TMF simulation

In order to compare the varying deformation behavior of the three material models described in chapter 2.3, the TMF test, subject to the load conditions as described before, was simulated by an anisothermal transient FEA. Besides thermo-physical properties, the material-dependent parameter sets required for each model were determined especially by using an experimental database from both isothermal strain-controlled LCF tests and time-to-rupture tests to adjust the hardening and viscous deformation behavior. The LCF tests were conducted at a constant strain rate $d\varepsilon=10^{-3}s^{-1}$ on smooth specimens by applying symmetric triangular shaped cycles fully reversed without dwell period. The database includes also a family of creep curves within the temperature range 400-800°C.

The stress response as a result of the TMF simulation by using the "elastoplastic" (ep), "elastoplastic & creep" (epc) and "viscoplastic" (vp) material model is shown in Figure 5, in which the 10th cycle after numerical and cyclic stabilization is plotted. These stress vs. time sequences are compared to the measured stress history (experimental) of the cyclic stabilized material condition at mid-life. The "viscoplastic" model provides the best stress approximation during the heating-up phase from the start of the cycle to approx. 300s compared to the "elastoplastic" and "elastoplastic & creep" model. Only the stress peak before stress relaxation is slightly overestimated. But when cooling down there is a significant difference in the shape of the stress curve for each model compared to the experimental result, whereas the shape of each model is the same at different stress levels.

For better understanding this discrepancy, the thermal strain caused by the temperature profile is analyzed. As can be seen in Figure 6, there is also after approximately 300s a remarkable difference between experimental and simulated thermal strain. The latter is calculated by applying the linear coefficient of thermal expansion which is determined on the basis of dilatometer tests for several sampling temperatures.

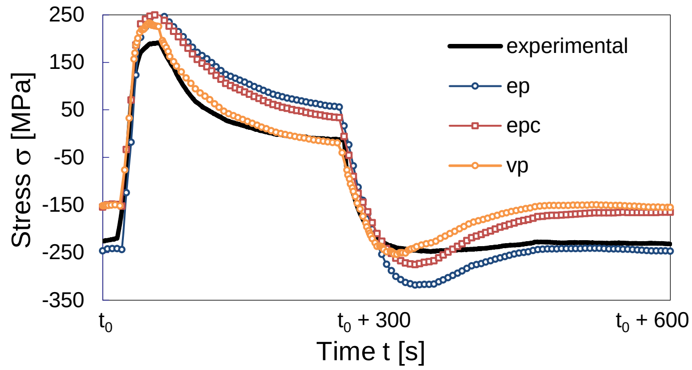

Figure 5. Stress vs. time sequence as result of TMF simulation by applying different kind of material models.

Obviously, the material batch used to manufacture the TMF specimens exhibits a different thermal expansion behavior, especially in the temperature range from approx. 300°C to 500°C, compared to the material batch used to determine thermal expansion coefficients. Thus, different thermal strains cause different mechanical strains in which the elastic part is responsible for stress calculation. The elastic strain portion is also influenced by the inelastic strain which differs in relation to the material model.

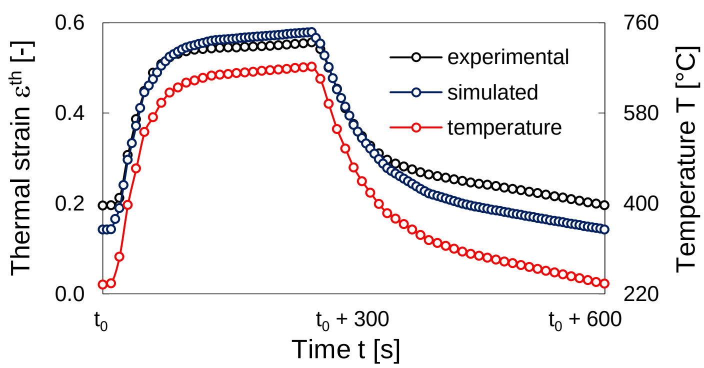

Figure 6. Thermal strain vs. time sequence by comparing experimental and simulated result with respect to acting temperature throughout the entire TMF cycle.

3.3 TMF damage evaluation

Following Equation (11) by applying the underlying numerical calculation method, creep damage fraction and fatigue damage fraction until crack initiation were determined by use of a representative cycle at mid-life on basis of the TMF tests conducted; the results are shown in Figure 7 in which each square represents a repeatable test. This assumption is justified due to minor hardening and softening effects during TMF loading of the investigated material D5S. Both damage fractions are approximately in the same range.

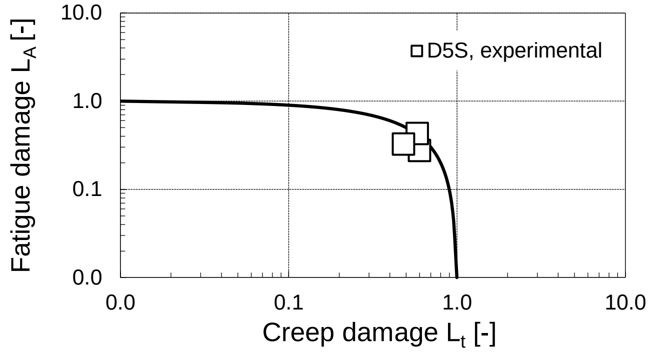

Figure 7. Fatigue and creep damage fractions of D5S specimens under characteristic TMF load conditions.

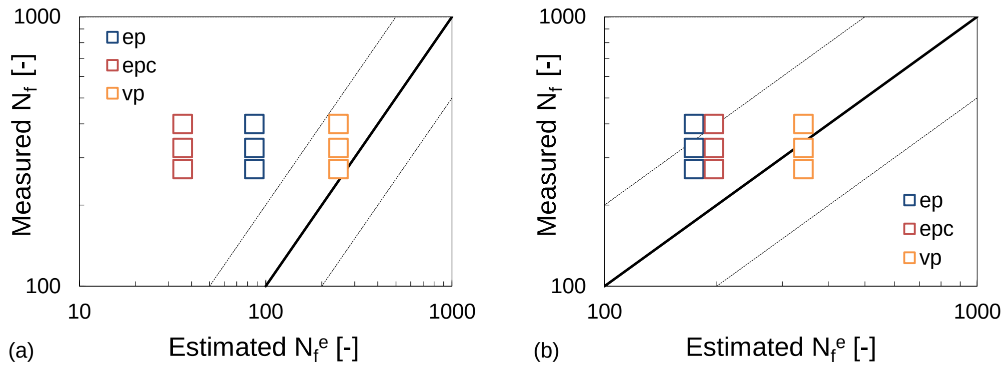

Figure 8. Recalculated cycle numbers until crack initiation N_f^e of TMF tested specimens by applying different kind of material models (a) without and (b) with backstress correction within the damage calculation procedure.

By applying the mean creep-fatigue damage sum L derived from Figure 7, the recalculation of the cycle numbers until crack initiation N_f^e provides the lifetime estimation of TMF tested specimens shown in Figure 8 as a function of the different kind of material models applied in the preceding TMF simulation. The results are compared to measured values N_f, whereby each square represents again a repeatable test. In Figure 8 (a) the recalculation is done without, and in Figure 8 (b) with backstress correction, which means that the backstress is subtracted from the FEA resultant stress at each time step to obtain the effective acting stress inside the stress-strain hysteresis loop. Both the “elastoplastic” and the “elastoplastic & creep” model are strongly conservative in their estimations without backstress correction. Results can be shifted towards the conventional scatter band of the scale of 2 by considering backstress correction. In contrast to that, the “viscoplastic” model shows in both cases results within the scatter band, whereby the backstress correction enables estimations in excellent agreement with experimental crack initiations, Figure 8 (b).

4. Conclusion

The plasticity models proposed are capable to describe the thermo-mechanical material behavior under complex variations of temperature and strain, whereby the rate-independent formulation is reasonable as long as the plastic deformation process induces low strain rates. The resulting stress and strain state of each model is of adequate accuracy for subsequent damage assessment as demonstrated on smooth specimens subject to characteristic load conditions. This trend also highlights the potential of the damage calculation procedure.

Nevertheless, the viscoplastic model shows its advantage especially in describing the deformation behavior. Besides numerical efficiency the minimization of material parameters required has been focused during the evaluation. The adaption for T/H design is still being investigated at which the computational efficiency also needs to be proven. Ideally, there should be no remarkable loss in computational time compared to both other models presented.

To confirm the damage fractions of creep and fatigue, additional metallurgical investigations on the microstructure are necessary to separate the damage mechanism and to determine the damage fractions quantitatively, e.g. by detecting persistent slip bands, creep pores on grain boundaries and disconnections/cracks between grain boundaries. Alternative fatigue damage methods, e.g. based on micro crack growth, and refinements in order to describe creep characteristics are also being focused on enabling the flexibility of mechanism-based damage calculation.

5. References

1. Abaqus Theory Manual, Version 6.10-1, Dassault Systèmes Simulia Corp., Providence, RI.
2. Armstrong, P.J. and C.O. Frederick, “A mathematical representation of the multiaxial Bauschinger effect”, CEGB Report RD/B/N 731, Berkeley Nuclear Laboratories, 1966.
3. Chaboche, J.L., “Time-independent constitutive theories for cyclic plasticity”, Int J Plast 2, p. 149-188, 1986.

4. Chaboche, J.L., “Constitutive equations for cyclic plasticity and cyclic viscoplasticity”, Int J Plast 5, p. 247-302, 1989.
5. Garofalo, F., “Fundamentals of creep and creep-rupture in metals, Macmillan, New York, 1965.
6. Laengler, F., Mao, T. and A. Scholz, “Validation of a phenomenological lifetime estimation approach for application on turbine housings of turbochargers”, 9th Int. Conf. on Turbochargers and Turbocharging, May 19-20, London, p. 193-205, 2010a.
7. Laengler, F., Mao, T. and A. Scholz, “Phenomenological lifetime assessment for turbine housings of turbochargers”, 9th Int. Conf. on Multiaxial Fatigue & Fracture, June 7-9, Parma, 2010b.
8. Laengler, F., Mao, T. and A. Scholz, “Investigation of application-specific phenomena to improve the lifetime assessment for turbine housings of turbochargers”, Procedia Engineering 10, p. 1163-1169, 2011a.
9. Laengler, F., Mao, T. and A. Scholz, “Influence analysis of application-specific phenomena on the creep-fatigue life for turbine housings of turbochargers”, J. ASTM Intl., Vol.9, No.3. doi: 10.1520/JAI103945, 2012.
10. Larson, F.R. and J. Miller, “A time-temperature relationship for rupture and creep stress”, Trans. ASME 74, p.76, 1952.
11. Miner, M.A., “Cumulative Damage in Fatigue”, J Appl Mech 12, A1S9, 1945.
12. Norton, F.H., “The creep of steel at high temperature”, New York: McGraw Hill; 1929.
13. Scholz, A. and C. Berger, “Deformation and life assessment of high temperature materials under creep fatigue loading”, Materialwissenschaft und Werkstofftechnik 36, p. 722-730, 2005.
14. Taira, S., “Lifetime of structures subjected to varying load and temperature”, In: Hoff, N.J., editor, Creep in Structures, New York: Academic Press; p. 96-119, 1962.